catalysts

MDPI

Article

Real-Time UV/VIS Spectroscopy to Observe Photocatalytic Degradation

Sanguk Woo, Hyein Jung and Yohan Yoon *

Department of Materials Engineering, Korea Aerospace University, Goyang 10540, Republic of Korea
* Correspondence: yyoon@kau.ac.kr; Tel.: +82-2-300-0162

Abstract: In this work, we have developed a real-time UV/VIS spectroscopy method using a broadband Xenon Arc lamp to detect photocatalytic reactions in real time. A CMOS camera was used instead of an output slit to capture all spectral information simultaneously, which can enable a real-time detection of the UV/VIS absorption of the analytes within a single frame of the camera. To verify real-time spectroscopy, a wavelength calibration process was performed using three laser line filters and a didymium glass filter sample. To demonstrate that this real-time spectroscopic setup can be used for rapid measurements, MB samples were used to observe the real-time photocatalytic degradation of MB by TiO_2 nanoparticles. For real-time measurement, four samples with different TiO_2 nanoparticle quantities showed different photocatalytic degradation mechanisms. By plotting the spectra every 20 ms, the series of spectra clearly showed the degradation of MB in real time.

Keywords: real-time; UV/VIS spectroscopy; photocatalytic degradation; broadband light

1. Introduction

Real-time spectroscopic techniques, spanning from ultraviolet (UV) to infrared (IR) wavelengths, have been widely used to investigate physical and chemical mechanisms in various research areas, such as photonics [1,2], chemicals [3,4], and biomedical instruments [5,6]. In our previous study [7], we successfully demonstrated the feasibility of using a grating-based simultaneous spectroscopic technique with a broadband IR source to detect various types of chemical analytes in real time. This proof-of-concept approach can be extended to the UV/VIS spectral region, which is a conventional analytical chemistry technique for determining chemical analytes. Real-time UV/VIS spectroscopy offers the advantage of providing valuable information on the evolution of fast dynamic processes, including electronic transitions [8] and compositional changes [9], which are not easily accessible using conventional UV/VIS spectroscopy that requires wavelength tuning. Therefore, by employing real-time UV/VIS spectroscopy, it is possible to obtain a more comprehensive understanding of the physical and chemical mechanisms underlying a given process, as well as to uncover previously unknown features of the system under study.

Photocatalysis has become an area of immense interest due to its versatility in a range of reactions, including oxidation and dehydrogenation for organic degradation [10], air purification [11], and water detoxification [12]. Among the many pollutants, methylene blue (MB) is a major water contaminant and has been the focus of numerous studies on photocatalytic degradation of organic dyes [13]. A range of photocatalysts, such as TiO_2 nanoparticles [14], ZnO [15], and $CaIn_2O_4$ [16], have been studied for MB degradation. Among these, TiO_2 has emerged as the most promising candidate due to its high reaction rate. Since the reaction rate is a key factor in reducing the cost of photocatalytic processes, significant efforts have been invested in accelerating the reaction speed [17,18]. This underscores the importance of understanding the mechanisms of MB degradation and how they relate to the photocatalytic properties of TiO_2 nanoparticles.

Citation: Woo, S.; Jung, H.; Yoon, Y. Real-Time UV/VIS Spectroscopy to Observe Photocatalytic Degradation. *Catalysts* **2023**, *13*, 683. https://doi.org/10.3390/catal13040683

Academic Editor: Kangle Lv

Received: 28 February 2023
Revised: 21 March 2023
Accepted: 30 March 2023
Published: 31 March 2023

As the photocatalytic degradation rate of MB increases, it becomes increasingly important to employ in situ real-time spectroscopic methods to understand the degradation process, which can occur within sub-seconds. Although conventional UV/VIS spectroscopy [19] has been utilized to investigate the photocatalytic degradation mechanisms of MB, since its absorbance peaks are within the visible range, the real-time spectroscopic approach offers a more comprehensive understanding of the mechanism and enables the detection of peak position shifts of new peaks on a sub-second timescale, which are not easily accessible using conventional UV/VIS spectroscopy [20].

In this study, we present a novel approach for real-time spectroscopic detection of photocatalytic effects in samples using a broadband UV-enhanced Xenon Arc light source. Unlike conventional UV/VIS spectroscopy, our spectrometer captures the spectrally broadband light directly reflected from the grating using a CMOS camera, eliminating the need for a traditional output slit. This enables the real-time monitoring of all spectral information, including those that may be missed by traditional UV/VIS spectrometers. Moreover, our spectroscopic technique allows for simultaneous acquisition of spatial and spectral information, making it possible to monitor any inhomogeneous spatial variations of samples in real time.

The integration time of the CMOS camera sets the limit for the speed of our proposed technique, making it a fast and efficient method for real-time spectroscopy. Additionally, this protocol can be applied to any other spectroscopy that requires hyperspectral imaging in real time, making it a versatile and valuable tool for various scientific research [21,22]. Overall, our approach presents a significant advancement in the field of real-time spectroscopy, providing a powerful tool for monitoring fast dynamic processes in various scientific areas.

The development of our proposed real-time spectrometer represents a major advancement in the study of photocatalytic effects, with broad-reaching applications in environmental science, material science, and biomedical research. By enabling the real-time detection of photocatalytic effects, our spectrometer can play a pivotal role in optimizing photocatalytic processes and enhancing our understanding of their underlying mechanisms. The ability to simultaneously obtain spatial and spectral information is especially valuable in illuminating the heterogeneity of samples, which is often a key factor in photocatalysis. Our real-time spectroscopic technique has the potential to revolutionize the field of spectroscopy, leading to new scientific discoveries and facilitating breakthroughs in a range of disciplines. With its speed and versatility, this method promises to be a powerful tool for researchers seeking to unravel the mysteries of photochemical reactions and other dynamic phenomena.

2. Results

2.1. Optical Setup

In Figure 1, we present a detailed schematic of our real-time spectroscopy setup, which harnesses the broadband Xenon Arc lamp described in the Experimental Section to enable the detection of all spectral information of dispersed broadband light sources from a grating using a complementary metal-oxide semiconductor (CMOS) camera [7]. Our technique employs a Xenon Arc lamp as a broadband light source, which is focused into a vertical slit with a width of 100 μm using two plano-convex lenses. The light then passes through the sample, illuminates a grating with a groove density of 1200 grooves/mm, and the dispersive spectrum is recollimated by the second off-axis parabolic mirror (OAP). To prevent the CMOS camera from receiving saturated data, we employed neutral density (ND) filters (optical density = 1.0, transmission = 10%) before capturing the light beam. Overall, our setup offers a robust and efficient solution for real-time spectroscopy with the potential to advance a variety of scientific fields.

Our real-time spectroscopy setup not only provides real-time detection of photocatalytic effects, but also offers numerous advantages over traditional UV/VIS spectroscopy techniques. The use of a broadband Xenon Arc lamp allows for the detection of all spectral information, which can be crucial for understanding complex reaction mechanisms. In

addition, the direct capture of the spectrally broadband light reflected from the grating using a CMOS camera eliminates the need for a traditional output slit, simplifying the setup, and reducing the potential for signal loss. This unique feature allows for the real-time monitoring of inhomogeneous spatial variations of samples, which is particularly useful for the study of photocatalysis, where spatial heterogeneity is often a critical factor in determining reaction kinetics. Overall, our real-time spectroscopy setup represents a significant advancement in the field of spectroscopy and has the potential to drive new discoveries in a wide range of scientific disciplines.

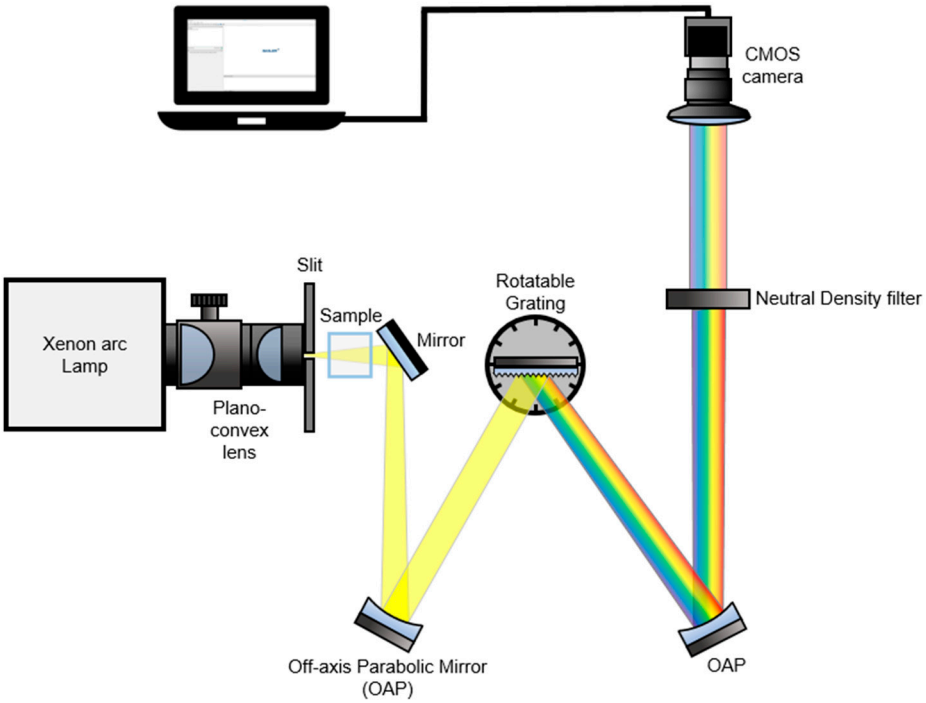

Figure 1. A schematic of the real-time UV/VIS spectroscopy setup. Broadband "white" light having a UV to NIR wavelength range was used as an illumination source. The light beam passed through a sample is collimated by an off-axis parabolic mirror (OAP) and it illuminates a grating. The dispersive spectrum is recollimated and passed through a neutral density (ND) filter (1.0 optical density, 10% transmission). A dispersed broadband signal is captured by a CMOS camera.

2.2. Wavelength Calibration

In this study, we utilized the developed real-time spectrometer to generate two-dimensional contour maps of the broadband light source signal captured by the CMOS camera, as demonstrated in Figure 2a–c. The contour maps contain both spectral and spatial information of the dispersive light source from the grating, with the X-axis and Y-axis camera pixels representing spectral and spatial information, respectively. To obtain the spectral information of the emission signal, we performed a pixel-to-wavelength conversion process using three laser line filters (center peaks of 488, 532, and 632.8 nm) placed in the optical path of the CMOS camera to mark the specific wavelengths on the contour maps. Each laser line filter had a full width at half maximum (FWHM) value of 1 ± 0.2 nm. A representative contour map, combining the three different emission signals obtained by using the laser line filters, is illustrated in Figure 2b, with the three emission peaks extracted from the white line shown in Figure 2d. The peak positions of the three spectra have a linear relationship with the wavelength of the broadband light source, as demonstrated in Figure 2e. By utilizing this positive correlation, we successfully completed the pixel-to-wavelength process, as shown in Figure 2c,f. Each contour map shows a region of interest (ROI) by windowing down to a size of 300×300 pixels, which provides the highest-quality image for the light-illuminated region. The contour maps of the emission spectra

in Figure 2 only have a wavelength range of 500 nm to 680 nm, where the spectrum of the MB sample is present. We intentionally selected this wavelength range to focus on the dispersive spectrum of MB using bandpass filters. However, the wavelength range or center wavelength can be adjusted by using other bandpass filters or rotating the grating, depending on the absorption spectra of the analytes. The ability to obtain such detailed and versatile information through our real-time spectrometer can greatly enhance the understanding and optimization of photocatalytic processes in various fields.

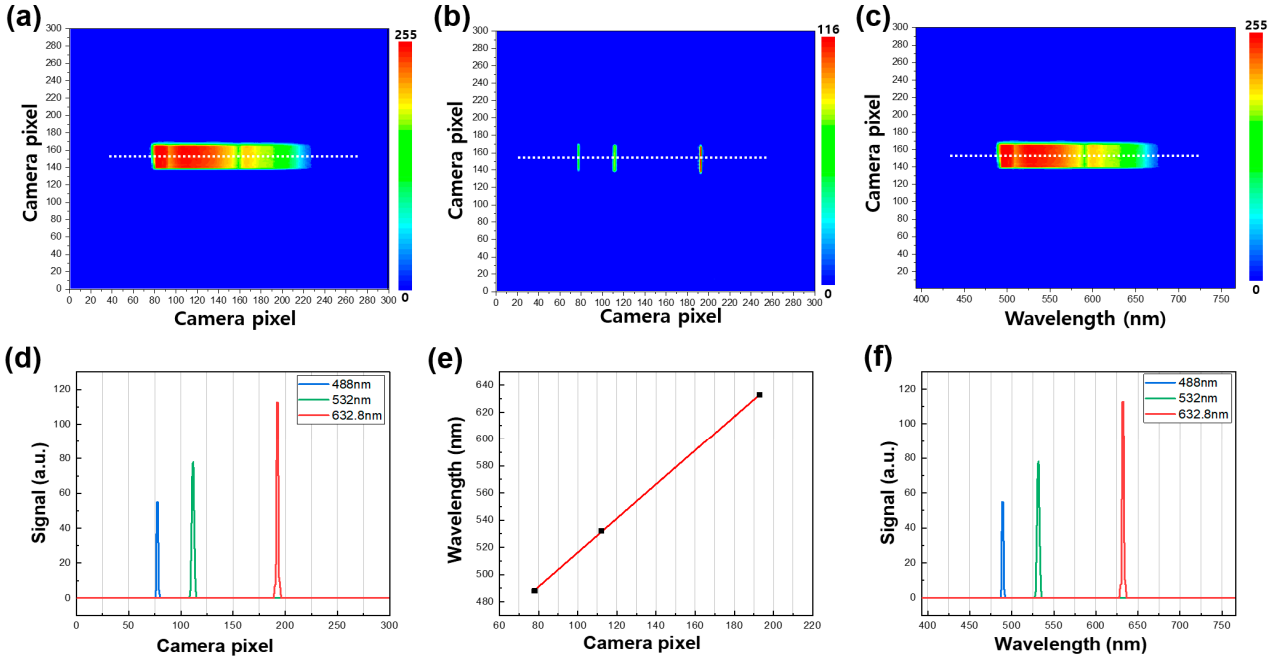

Figure 2. (**a**) A representative contour map of the broadband light source in the wavelength range of 500 nm to 680 nm. (**b**) A representative contour map combining three different emission signals was obtained by using the three laser line filters (488 nm, 532 nm, and 632.8 nm, left to right). (**c**) A representative contour map of the broadband light source after the wavelength conversion process. (**d**) Emission spectra of the white line in (**b**). (**e**) Correlation of the X camera pixel with wavelength. (**f**) Emission spectra of the white line in (**b**) after the wavelength conversion process.

In order to evaluate the accuracy of the wavelength calibration process, we performed an experiment using a didymium glass filter as a reference sample, which has characteristic peaks in both the ultraviolet and visible ranges. A representative contour map of the broadband light source passing through the didymium glass filter was obtained and is shown in Figure 3a. We recorded the raw spectra of both the broadband light source (black line in Figure 3b) and the didymium glass filter sample (blue line in Figure 3b). The absorbance spectrum of the didymium glass filter sample (black line in Figure 3c) was then acquired by dividing its spectrum by the reference spectrum (broadband source), as shown in Figure 3c. We further compared the absorbance spectrum obtained using our real-time UV/VIS measurement setup with the one obtained using a commercial UV/VIS spectrometer that requires continuous wavelength tuning while acquiring a spectrum. The two absorbance spectra agreed well, except for a distinctive absorbance feature present in the 560–610 nm wavelength range of the real-time UV/VIS measurement. This feature is attributed to two distinct peaks observed at 574 and 587 nm, which have previously been observed by other groups [23,24]. It is important to note that the peak position and spectral bandwidth of these two peaks may vary with the experimental setup. Overall, the results show that our real-time UV/VIS measurement setup provides accurate wavelength calibration, with only minor differences from a commercial spectrometer, and is therefore a reliable tool for acquiring accurate absorbance spectra.

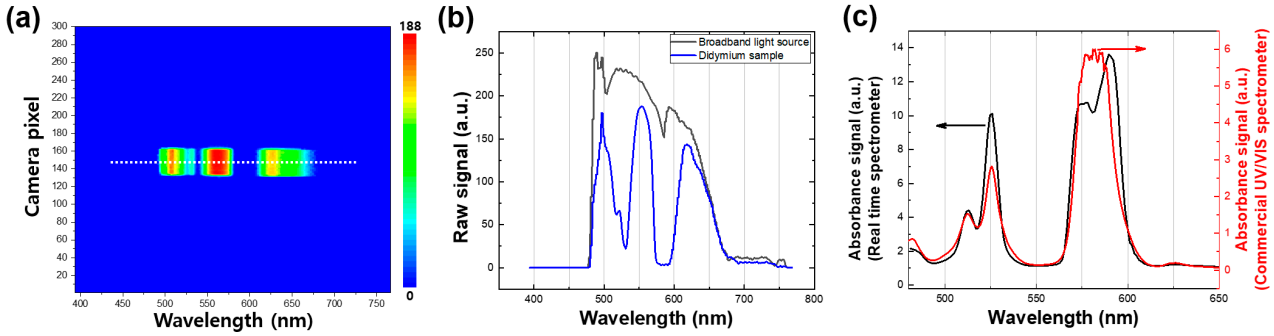

Figure 3. (**a**) A representative contour map of the broadband light source when the light passed through the didymium glass filter. (**b**) Emission spectra of the broadband light source (black) from the white line in Figure 2a. and the light source passed through the didymium sample (blue) from the white line in (**a**). (**c**) Absorbance spectrum of the didymium glass filter sample obtained by the real-time spectroscopy (black) and the spectrum obtained by the commercial UV/VIS spectroscopy (red).

To obtain accurate and reliable results in real-time spectroscopy, it is paramount to optimize the input slit aperture size. The choice of this parameter has a significant impact on both the spectral resolution and the signal-to-noise ratio of the absorbance spectra. Nevertheless, selecting the optimal slit aperture size can be challenging because using a narrow-slit aperture results in a high spectral resolution but yields a weak beam intensity, which in turn adversely affects the signal-to-noise ratio. Conversely, using a wider slit aperture enhances the beam intensity but results in lower spectral resolution. Therefore, the selection of the most appropriate slit aperture size is crucial. In our study, we have empirically determined the optimal slit aperture size of 10 µm, which provides sufficient spectral resolution and signal-to-noise ratio to effectively observe the absorbance spectra of MB samples. Although we did not elaborate on the experimental details of how we arrived at this optimum slit aperture size, we have ensured that our chosen size meets the requirements of the real-time spectroscopy setup to generate high-quality results.

2.3. Real-Time Sample Detection

The real-time spectroscopic technique discussed in the previous section offers a key advantage over traditional spectroscopic techniques. Its main benefit is the ability to simultaneously detect analyte absorption and chemical reactions, making it a powerful tool for monitoring chemical reactions in real time. Moreover, the technique has the potential for much faster sampling rates, which can be achieved by using faster frame rates and shorter integration times of the camera. However, the quality of each spectrum obtained is determined by the specification of the camera, which serves as the limiting factor. In this study, a camera frame integration time of 500 µs and a frame rate of 155 fps were used, providing satisfactory results. By adjusting these parameters, it is possible to further increase the sampling rate, provided that the signal-to-noise ratio remains adequate to obtain accurate sample spectra.

In this section, we employed a real-time spectroscopic setup to monitor the photodegradation of methylene blue (MB) by TiO_2 nanoparticles through photocatalysis, a widely adopted approach that exploits a photocatalyst to break down organic pollutants in the presence of light. Spectroscopic techniques, such as UV/VIS spectroscopy, were utilized to monitor the degradation process by measuring changes in the absorbance of MB as it was degraded by the photocatalyst. With the real-time spectroscopic setup, the MB degradation could be monitored in real time, and valuable information about the kinetics of the degradation process was obtained.

To demonstrate the effectiveness of the real-time spectroscopic setup, Figure 4a,b depict representative contour maps of the broadband light source when passing through the reference sample, consisting of TiO_2 nanoparticles in ethanol, and the MB sample, respectively. These contour maps provide a comprehensive graphical representation of the

spectral intensity of the broadband light source at various wavelengths, allowing for the identification of spectral changes over time. In Figure 4c, a representative absorbance contour map of the MB sample is presented, which was generated by subtracting the contour map of the reference broadband light source from that of the MB sample. The absorbance contour map provides a visual representation of the changes in the absorbance values of the MB sample over time. To further investigate these changes, Figure 4d illustrates the raw spectra extracted from the white dotted lines in the contour maps of the broadband light source, as a reference signal (black line) and for the MB sample (blue line), enabling the identification of spectral changes over time. These findings demonstrate the usefulness of the real-time spectroscopic setup in identifying and monitoring the degradation of MB by TiO_2 nanoparticles, providing valuable information about the kinetics of the degradation process.

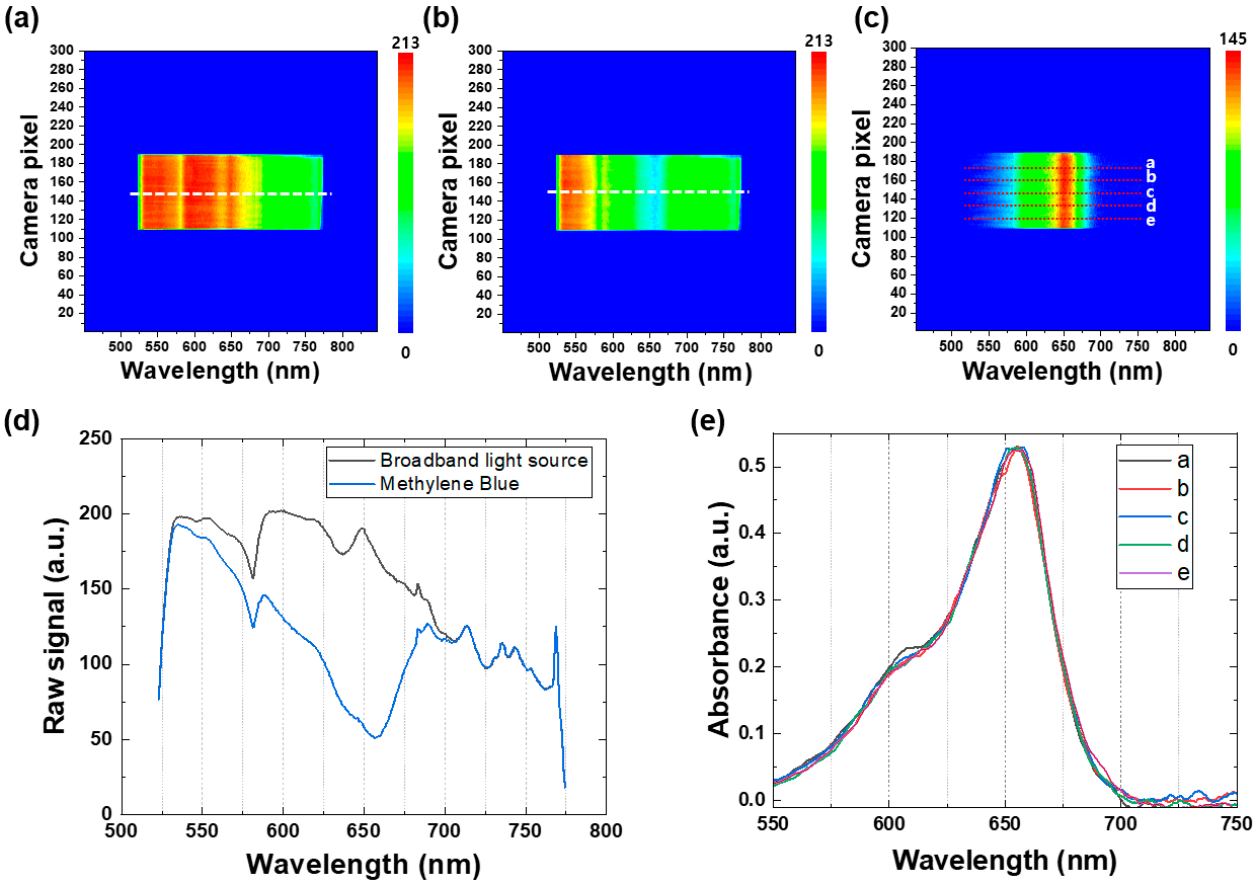

Figure 4. Representative contour maps of the broadband light source when the light passes through (**a**) the reference sample (TiO_2 nanoparticles in ethanol) and (**b**) the MB sample. (**c**) A representative absorbance contour map of the MB sample obtained by subtracting the contour map of the reference broadband light source. (**d**) Raw spectra extracted from the white dotted lines in the contour maps of the broadband light source (**a**,**b**) as the reference signal (black line) and the MB sample (blue line). (**e**) Absorbance spectra of the MB sample extracted from five different white dotted lines in the absorbance contour map (**c**).

Figure 4e displays the absorbance spectra of the MB sample extracted from five different white dotted lines in the absorbance contour map (see Figure 4c). It is noteworthy that the Y-axis (camera pixel) represents the spatial information of the samples, enabling observation of any spatial variation in the light-illuminated area of the samples. In this study, all the MB samples were homogeneous mixtures containing uniformly distributed TiO_2 nanoparticles, and no significant spatial variation in the five different spectra was observed, as illustrated in Figure 4e. This feature is particularly advantageous over other commercial

in situ spectroscopic techniques, as the real-time spectroscopy employed in this study is beneficial for obtaining spatial and spectral information of any inhomogeneous mixture samples or non-uniform thin-film samples in real time, which makes it an invaluable tool for researchers working with complex samples.

Figure 5a–d illustrate distinct photocatalytic degradation rates that are dependent on the quantity of TiO_2 [25]. Sample A, which contains the lowest amount of TiO_2 (0.003 wt.%), showed a relatively slow degradation rate of 30% over 10 min. However, as the quantity of TiO_2 increased to 0.006 wt.%, the degradation rate increased to 50% over the same time period (Figure 5b). When the TiO_2 quantity was further increased to 0.010 wt.% (Figure 5c), the photocatalytic degradation rate of MB significantly accelerated, and a substantial drop in absorbance peaks (≈95% photocatalytic degradation) occurred within the first minute. The photocatalytic degradation rate remained almost the same even when the TiO_2 quantity was increased to 0.013 wt.%, indicating that the amount of TiO_2 required for the degradation of MB was saturated. By comparing Sample C and Sample D using Figure 5e,f, it is apparent that Sample D exhibited a lower amount and rate of degradation. This behavior can be attributed to an excessive amount of photocatalyst, which leads to several negative effects on the photocatalytic reaction. Firstly, an excess of photocatalyst can interfere with light transmission, thereby hindering the reaction. Secondly, excessive photocatalyst may aggregate and reduce the reaction surface area available to the substance being degraded. Thirdly, unbound photocatalysts may absorb energy required for bound photocatalysts to react, reducing the reaction efficiency. Finally, photo-excited photocatalysts may collide with ground-state photocatalysts, leading to a decreased reaction efficiency. To compare the photolysis phenomenon of the four different samples, Figure 5e,f illustrate changes in the absorption of 662 nm, which is the peak with methylene blue characteristics, and 603 nm, which is the shoulder. The peak of MB is due to the presence of S and N in the π-π bonds of the benzene ring, while the shoulder is caused by the vibration transition in the ground state and the excited state [26]. We can obtain valuable information about benzene ring cracking through the 662 nm peak, which represents the absorption due to S and N in the π-π bonding of the benzene ring. Based on our results, the bleached sample showed approximately 95% degradation, while TiO_2 amounts of 1 mg, 2 mg, 3 mg, and 4 mg each exhibited a reduction in absorbance of 28%, 43%, 97%, and 92%, respectively. These findings suggest that the degree of benzene ring cracking due to reduction is dependent on the amount of photocatalyst used.

Table 1. Four different MB samples with TiO_2 nanoparticle concentrations.

Sample	Ethanol (mL)	Methylene Blue (mg)	TiO_2 Nanoparticle (mg)	TiO_2 Nanoparticle (wt.%)
Sample A	40	0.2	1	0.003
Sample B	40	0.2	2	0.006
Sample C	40	0.2	3	0.010
Sample D	40	0.2	4	0.013

It is important to note that the temporal resolution of this condition (1 min) is comparable to that of conventional UV/VIS spectroscopy, which is insufficient to capture rapidly changing spectra, as in this case. Figure 5e,f show that the information on the photocatalytic degradation mechanism was insufficient during the first minute. However, the real-time spectroscopic approach used in this study enabled the continuous monitoring of the spectral changes in the sample with high temporal resolution, allowing us to capture detailed information on the degradation mechanism that conventional spectroscopic techniques cannot provide.

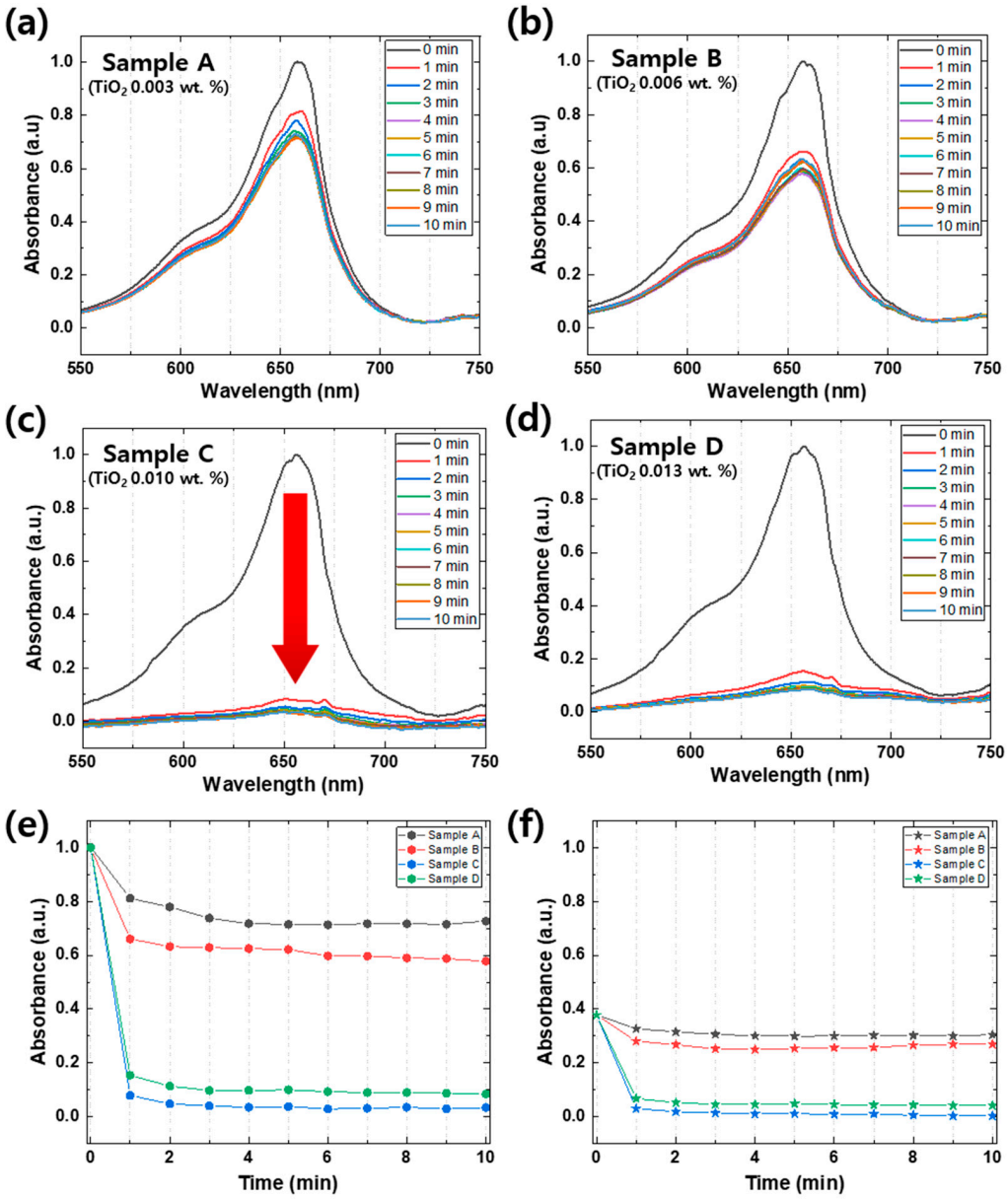

Figure 5. (**a**–**d**) Absorbance spectra of 4 different MB samples (Samples A to D) with TiO_2 nanoparticle concentration, which is described in Table 1. The arrow in (**c**) indicates rapid photodegradation occurring within 1 min, from 0 min to 1 min. Changes in the absorption of 662 nm (**e**), which is the peak with methylene blue characteristics, and 603 nm (**f**), which is the shoulder at intervals of 1 min per 10 min of 4 different samples. The black lines, the red lines, the blue lines, and the green lines are Samples A, B, C, and D, respectively.

Real-time spectroscopy is a powerful technique for providing a comprehensive understanding of photocatalytic degradation mechanisms, particularly regarding temporal variation and peak-to-peak intensity changes. In this study, Sample C showed the most rapid degradation of MB, with a significant drop in absorbance peaks within the first 10 s. Figure 6a illustrates a series of spectra of Sample C taken at 20-millisecond intervals for the first 10,000 milliseconds, providing a detailed look at the degradation process. As shown in Figure 6b, the 603 nm shoulder, which represents absorption by vibration of methylene blue, rapidly decreased at the beginning and bleached at 10,000 milliseconds, while the peak of 662 nm, which represents absorption by S and N in the π-π bonds of the benzene ring, was gradually reduced and decomposed by nearly 75% at 10,000 milliseconds. These results provide further insights into the degradation mechanism and highlight the

potential of real-time spectroscopy in detecting any peak position shifts of new peaks on a sub-second timescale, which cannot be observable in Figure 5, where only the suppression of the absorbance peaks is evident. Therefore, real-time spectroscopy is a valuable tool for obtaining detailed information about chemical reactions and mechanisms.

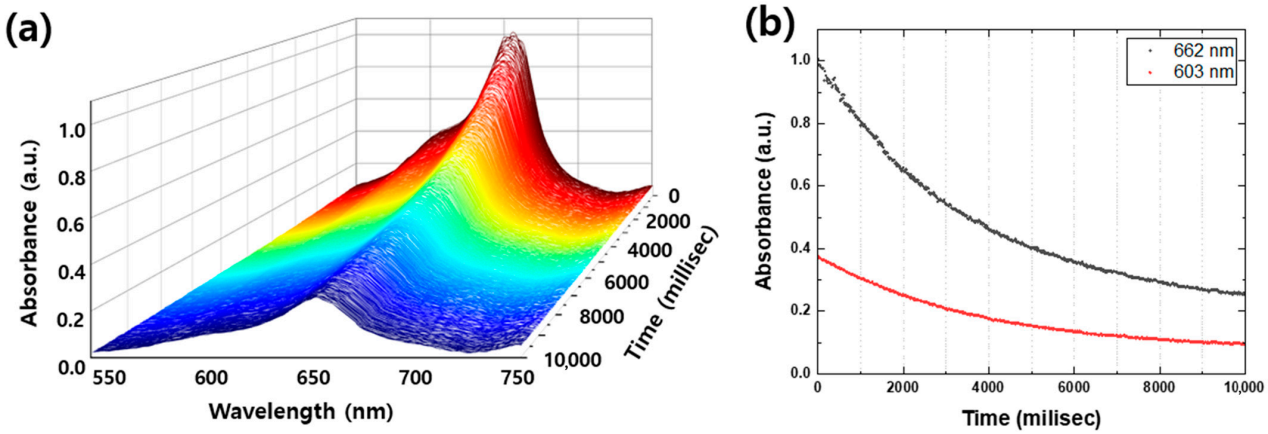

Figure 6. (**a**) Absorbance spectra of Sample C for the first 10,000 milliseconds (millisec) in every 20 millisec. (**b**) Photodegraded MB peak and shoulder per 20 millisec of 4 different samples. The black dots and the red dots are the MB peak (662 nm) and the shoulder (603 nm), respectively.

3. Materials and Methods

3.1. UV/VIS Spectroscopy

A UV/VIS/NIR infrared (NIR) spectrophotometer (Shimadzu, UV-3600, Kyoto, Japan) was used to obtain a reference UV/VIS absorbance spectrum for comparison with that of real-time UV/VIS spectroscopy. The absorbance of the sample was calculated using the following equation:

$$A = -\log_{10} T = \log_{10} \frac{I_0}{I} \quad (1)$$

where A is the absorbance, T is the transmittance, I_0 is the intensity of transmitted light, and I is the intensity of incident light [27]. UV/VIS spectroscopy was performed in the wavelength range of 400 to 800 nm, where the MB absorbance peaks exist.

3.2. Xenon Arc Lamp Light Source

We used a commercially available UV-enhanced Xenon Arc lamp (Newport, 6269) to obtain a broadband UV/VIS spectrum containing an intensive 365 nm for electron excitation of TiO_2 nanoparticles [25]. To achieve a rapid degradation rate of MB, the lamp power was fixed at the maximum power (1000 W). The lamp was packaged using a housing (Newport, 66921) for the cooling system and light collimation. Two plano-convex lenses were used to collimate and focus the incoherent beams.

3.3. Sample Preparation

To calibrate the wavelength for real-time spectroscopy, we employed a commercially available didymium glass filter (Hellma, F7, Müllheim, Germany), which is commonly used for UV/VIS spectroscopy due to its sharp peak in the UV/VIS region [28]. For real-time spectroscopic measurements, we used MB samples dissolved in ethyl alcohol (ethanol). We prepared four MB samples with varying concentrations of TiO_2 nanoparticles by adding commercially available TiO_2 nanoparticles (Degussa, P-25) to the MB solution. Specifically, 0.8 mg of MB was dissolved in 160 mL of ethanol, sonicated for 40 min to ensure complete dissolution, and then divided into 4 samples. Different amounts of TiO_2 nanoparticles (1, 2, 3, and 4 mg) were added to each sample, which was then re-sonicated for 40 min to achieve particle dispersion [25,29]. The specific details are presented in Table 1. To conduct

the real-time UV/VIS spectroscopy measurements, the MB/TiO_2 samples were stored in quartz cuvettes.

3.4. TiO_2 Photocatalysis

TiO_2 nanoparticles are widely known as typical photocatalysts for the degradation of organic compounds [25]. This photocatalytic function is activated when TiO_2 nanoparticles are irradiated by 365 nm light, owing to the wide bandgap of TiO_2 nanoparticles [30]. Upon photoexcitation, excited electrons in TiO_2 nanoparticles can oxidize organics, and the complex oxidation mechanism has been described elsewhere [31]. Considering that MB is an organic dye that can be oxidized by TiO_2 nanoparticle photocatalysis, and its absorption peaks occur in the visible region, MB degradation is an ideal candidate for our new real-time spectrometer sample.

3.5. CMOS Camera

FPA with (5.86 × 5.86) µm pixels. The noise-equivalent temperature difference (NETD) was approximately 50 mK. The frame rate of the CMOS camera was 155 Hz for the full image (1920 × 1200), and the frame integration time was programmable from 20 µs to 10 s.

4. Conclusions

In this study, we developed a real-time spectrometer based on a grating system that operates in the UV/VIS spectrum region. To achieve this, we used a commercially available UV-enhanced Xenon Arc lamp as a light source due to its wide spectral width that can cover the UV to NIR range. This setup allowed us to record any changes in the spectral data of the sample in real time, without having to rotate the grating, by using a CMOS camera. This camera enabled the simultaneous detection of UV/VIS absorption of analytes within a single frame in real time.

Before conducting the sample measurement, we performed wavelength calibration using three laser line filters to convert one axis of the camera pixel to the wavelength. The pixel–wavelength match data demonstrated a linear relationship between the three laser line filters. To verify this conversion, we used a didymium glass filter, which is widely used as a calibration sample in UV/VIS spectrophotometry.

To demonstrate the applicability of this real-time spectroscopic setup for rapid measurements, we conducted a study on the photocatalytic degradation of MB by TiO_2 nanoparticles. Four samples with different amounts of TiO_2 nanoparticles (1 mg, 2 mg, 3 mg, and 4 mg) showed distinct photocatalytic degradation mechanisms. To observe the real-time degradation of MB, we plotted the spectra every 20 milliseconds for Sample C, which exhibited a dramatic peak change within a few seconds. The series of spectra showed the degradation of MB in real time, providing more details about the degradation mechanism, such as temporal variation of the degradation rate and peak-to-peak intensity change, etc.

Overall, the use of our real-time spectroscopy setup offers a rapid and efficient method for simultaneously obtaining valuable spectral and spatial information. Our technique holds significant potential for a wide range of scientific research, including environmental science, material science, and biomedical research. By enabling the real-time detection of all spectral information, our spectroscopy setup can aid in the optimization of photocatalytic processes and provide new insights into the underlying mechanisms of complex chemical reactions.

Author Contributions: Conceptualization, S.W. and Y.Y.; methodology, S.W. and H.J.; validation, all authors; formal analysis, S.W.; investigation, S.W. and Y.Y.; resources, Y.Y.; data curation, all authors; writing—review and editing, S.W. and Y.Y.; visualization S.W. and Y.Y.; supervision, Y.Y. All authors have read and agreed to the published version of the manuscript.

Funding: This work was supported by a National Research Foundation of Korea (NRF) grant funded by the Korea Government (MSIT) (No. NRF-2021R1F1A1063047). This study was supported by the K-Sensor Development Program (No. RS-2022-00154729) funded by the Ministry of Trade, Industry, and Energy (MOTIE, Republic of Korea).

Data Availability Statement: Not applicable.

Conflicts of Interest: The authors declare no conflict of interest.

References

1. Waterhouse, G.I.; Waterland, M.R. Opal and inverse opal photonic crystals: Fabrication and characterization. *Polyhedron* **2007**, *26*, 356–368. [CrossRef]
2. Ferraris, M.; Milanese, D.; Contardi, C.; Chen, Q.; Menke, Y. UV–Vis, FT-IR and EPR investigation on multi-component germano-silicate glasses for photonics. *J. Non-Cryst. Solids* **2004**, *347*, 246–253. [CrossRef]
3. Wang, J.; Burdzinski, G.; Kubicki, J.; Platz, M.S. Ultrafast UV−Vis and IR Studies of p-Biphenylyl Acetyl and Carbomethoxy Carbenes. *J. Am. Chem. Soc.* **2008**, *130*, 11195–11209. [CrossRef]
4. Kazarian, S.; Chan, K. Applications of ATR-FTIR spectroscopic imaging to biomedical samples. *Biochim. Biophys. Acta (BBA)-Biomembr.* **2006**, *1758*, 858–867. [CrossRef] [PubMed]
5. Kennis, J.T.; Groot, M.-L. Ultrafast spectroscopy of biological photoreceptors. *Curr. Opin. Struct. Biol.* **2007**, *17*, 623–630. [CrossRef]
6. Grupe, M.; Bäppler, F.; Theiß, M.; Busch, J.M.; Dietrich, F.; Volz, D.; Gerhards, M.; Bräse, S.; Diller, R. Real-time observation of molecular flattening and intersystem crossing in [(DPEPhos) Cu (i)(PyrTet)] via ultrafast UV/Vis-and mid-IR spectroscopy on solution and solid samples. *Phys. Chem. Chem. Phys.* **2020**, *22*, 14187–14200. [CrossRef]
7. Yoon, Y.; Breshike, C.J.; Kendziora, C.A.; Furstenberg, R.; McGill, R.A. Simultaneous real-time spectroscopy using a broadband IR laser source. *Opt. Express* **2021**, *29*, 8902–8913. [CrossRef]
8. Karabacak, M.; Cinar, M.; Unal, Z.; Kurt, M. FT-IR, UV spectroscopic and DFT quantum chemical study on the molecular conformation, vibrational and electronic transitions of 2-aminoterephthalic acid. *J. Mol. Struct.* **2010**, *982*, 22–27. [CrossRef]
9. Serezhkina, S.V.; Tyavlovskaya, E.A.; Shevchenko, G.P.; Rakhmanov, S.K. Investigation of structural and compositional changes in silver-doped GeO2 thin films. *J. Non-Cryst. Solids* **2005**, *351*, 35–40. [CrossRef]
10. Herrmann, J.-M. Photocatalysis. In *Kirk-Othmer Encyclopedia of Chemical Technology*; John Wiley & Sons, Inc.: Hoboken, NJ, USA, 2017; pp. 1–44.
11. Wen, M.; Li, G.; Liu, H.; Chen, J.; An, T.; Yamashita, H. Metal–organic framework-based nanomaterials for adsorption and photocatalytic degradation of gaseous pollutants: Recent progress and challenges. *Environ. Sci. Nano* **2019**, *6*, 1006–1025. [CrossRef]
12. Robert, D.; Malato, S. Solar photocatalysis: A clean process for water detoxification. *Sci. Total Environ.* **2002**, *291*, 85–97. [CrossRef] [PubMed]
13. Houas, A.; Lachheb, H.; Ksibi, M.; Elaloui, E.; Guillard, C.; Herrmann, J.-M. Photocatalytic degradation pathway of methylene blue in water. *Appl. Catal. B Environ.* **2001**, *31*, 145–157. [CrossRef]
14. Kwon, C.H.; Shin, H.; Kim, J.H.; Choi, W.S.; Yoon, K.H. Degradation of methylene blue via photocatalysis of titanium dioxide. *Mater. Chem. Phys.* **2004**, *86*, 78–82. [CrossRef]
15. Fan, H.; Zhao, X.; Yang, J.; Shan, X.; Yang, L.; Zhang, Y.; Li, X.; Gao, M. ZnO–graphene composite for photocatalytic degradation of methylene blue dye. *Catal. Commun.* **2012**, *29*, 29–34. [CrossRef]
16. Tang, J.; Zou, Z.; Yin, J.; Ye, J. Photocatalytic degradation of methylene blue on $CaIn_2O_4$ under visible light irradiation. *Chem. Phys. Lett.* **2003**, *382*, 175–179. [CrossRef]
17. Yang, X.; Chen, W.; Huang, J.; Zhou, Y.; Zhu, Y.; Li, C. Rapid degradation of methylene blue in a novel heterogeneous Fe_3O_4@ rGO@ TiO_2-catalyzed photo-Fenton system. *Sci. Rep.* **2015**, *5*, 1–10. [CrossRef]
18. Muniandy, L.; Adam, F.; Mohamed, A.R.; Ng, E.-P.; Rahman, N.R.A. Carbon modified anatase TiO_2 for the rapid photo degradation of methylene blue: A comparative study. *Surf. Interfaces* **2016**, *5*, 19–29. [CrossRef]
19. Singhal, G.; Rabinowitch, E. Changes in the absorption spectrum of methylene blue with pH. *J. Phys. Chem.* **1967**, *71*, 3347–3349. [CrossRef]
20. Xu, X.; Lei, M.; Huang, K.; Liang, C.; Xu, J.; Shangguan, Z.; Yuan, Q.; Ma, L.; Du, Y.; Fan, D. A facile route to porous beta-gallium oxide nanowires-reduced graphene oxide hybrids with enhanced photocatalytic efficiency. *J. Alloys Compd.* **2015**, *623*, 24–28. [CrossRef]
21. Yesilkoy, F.; Arvelo, E.R.; Jahani, Y.; Liu, M.; Tittl, A.; Cevher, V.; Kivshar, Y.; Altug, H. Ultrasensitive hyperspectral imaging and biodetection enabled by dielectric metasurfaces. *Nat. Photonics* **2019**, *13*, 390–396. [CrossRef]
22. Lu, G.; Fei, B. Medical hyperspectral imaging: A review. *J. Biomed. Opt.* **2014**, *19*, 010901. [CrossRef] [PubMed]
23. Shultz, A.; Campbell, D.; Messman, J. Reference material standardization guidelines for quality control and validation of UV/VIS absorption spectrophotometers. *Cal Lab* **1998**, *27*.
24. Didymium Glass Reference for Wavelength in the Visible. Available online: https://www.starnacells.com/d_ref/d_wl/DG.html (accessed on 17 May 2022).

25. Lakshmi, S.; Renganathan, R.; Fujita, S. Study on TiO_2-mediated photocatalytic degradation of methylene blue. *J. Photochem. Photobiol. A Chem.* **1995**, *88*, 163–167. [CrossRef]
26. Heger, D.; Jirkovsky, J.; Klan, P. Aggregation of methylene blue in frozen aqueous solutions studied by absorption spectroscopy. *J. Phys. Chem. A* **2005**, *109*, 6702–6709. [CrossRef]
27. Libowitzky, E.; Rossman, G.R. Principles of quantitative absorbance measurements in anisotropic crystals. *Phys. Chem. Miner.* **1996**, *23*, 319–327. [CrossRef]
28. Eckerle, K.; Chang, S.; Hsia, J. Calibration in 1976 and 1983 of didymium glass filters issued as NBS Standard Reference Materials. *Color Res. Appl.* **1985**, *10*, 32–37. [CrossRef]
29. Azeez, F.; Al-Hetlani, E.; Arafa, M.; Abdelmonem, Y.; Nazeer, A.A.; Amin, M.O.; Madkour, M. The effect of surface charge on photocatalytic degradation of methylene blue dye using chargeable titania nanoparticles. *Sci. Rep.* **2018**, *8*, 1–9. [CrossRef] [PubMed]
30. Umebayashi, T.; Yamaki, T.; Tanaka, S.; Asai, K. Visible light-induced degradation of methylene blue on S-doped TiO_2. *Chem. Lett.* **2003**, *32*, 330–331. [CrossRef]
31. Linsebigler, A.L.; Lu, G.; Yates, J.T., Jr. Photocatalysis on TiO_2 surfaces: Principles, mechanisms, and selected results. *Chem. Rev.* **1995**, *95*, 735–758. [CrossRef]